Lawrence Berkeley National Laboratory

Lawrence Berkeley National Laboratory

Title

A human breast cell model of pre-invasive to invasive transition

Permalink

https://escholarship.org/uc/item/88d6n6hf

Author

Weaver, Valerie M.

Publication Date

2008-03-10

Peer reviewed

A Human Breast Cell Model of Pre-invasive to Invasive Transition

Aylin Rizki[1†#], Valerie M. Weaver[2], Sun-Young Lee[1], Gabriela I. Rozenberg[2], Koei Chin[3], Connie A. Myers[1¶], Jamie L. Bascom[1], Joni D. Mott[1], Jeremy R. Semeiks[1], Leslie R. Grate[1§], I. Saira Mian[1], Alexander D. Borowsky[4], Roy A. Jensen[5], Michael O. Idowu[6], Fanqing Chen[1], David J. Chen[1,7], Ole W. Petersen[8], Joe W. Gray[1,4], Mina J. Bissell [1#]

[1]Life Sciences Division, Ernest Orlando Lawrence Berkeley National Laboratory, Berkeley, CA 94720. [2]Department of Pathology and Institute for Medicine and Engineering, University of Pennsylvania, PA 19104. [3]Department of Laboratory Medicine and Comprehensive Cancer Center, University of California, San Francisco, CA 94143. [4]Department of Pathology and Laboratory Medicine, and Center for Comparative Medicine, University of California, Davis. [5]Kansas Masonic Cancer Research Institute, Kansas City, KS 66160. [6]Department of Pathology, Virginia Commonwealth University, Richmond, VA 23298. [7]UT Southwestern Medical Center at Dallas 5323 Harry Hines Blvd, Dallas, Texas 75390. [8]The Panum Institute, DK-2200 Copenhagen N, Denmark.

[#]Corresponding authors: Mina J. Bissell, and Aylin Rizki[†], Life Sciences Division, Ernest Orlando Lawrence Berkeley National Laboratory. Address: One Cyclotron Road, Mailstop 977R225A, Berkeley CA 94720. Tel: (510) 486-4365, Fax: (510) 486-5586, email: MJBissell@lbl.gov, ARizki@vcu.edu. [†]Present address: Department of Radiation Oncology, Virginia Commonwealth University, Richmond, VA 23298. [¶]Present address: Department of Pathology and Immunology, Washington University, St. Loius, MO 63110. [§]Present address: Molecular, Cell, and Developmental Biology Department, University of California at Santa Cruz, Santa Cruz, CA 95064.

Abstract

A crucial step in human breast cancer progression is the acquisition of invasiveness. There is a distinct lack of human cell culture models to study the transition from pre-invasive to invasive phenotype as it may occur 'spontaneously' *in vivo*. To delineate molecular alterations important for this transition, we isolated human breast epithelial cell lines that showed partial loss of tissue polarity in three-dimensional reconstituted-basement membrane cultures. These cells remained non-invasive; however, unlike their non-malignant counterparts, they exhibited a high propensity to acquire invasiveness through basement membrane in culture. The genomic aberrations and gene expression profiles of the cells in this model showed a high degree of similarity to primary breast tumor profiles. The xenograft tumors formed by the cell lines in three different microenvironments in nude mice displayed metaplastic phenotypes, including squamous and basal characteristics, with invasive cells exhibiting features of higher grade tumors. To find functionally significant changes in transition from pre-invasive to invasive phenotype, we performed attribute profile clustering analysis on the list of genes differentially expressed between pre-invasive and invasive cells. We found integral membrane proteins, transcription factors, kinases, transport molecules, and chemokines to be highly represented. In addition, expression of matrix metalloproteinases MMP-9,-13,-15,-17 was up regulated in the invasive cells. Using siRNA based approaches, we found these MMPs to be required for the invasive phenotype. This model provides a new tool for dissection of mechanisms by which pre-invasive breast cells could acquire invasiveness in a metaplastic context.

Introduction

Breast carcinomas are phenotypically and behaviorally heterogeneous (1). Subtypes of breast cancer with distinct behavioral characteristics have been recognized morphologically as well as by molecular analyses. For all breast cancers, conversion to the invasive phenotype is distinct from metastasis but is an obligate prerequisite for metastasis thus representing a crucial step in cancer progression. Molecular profiling studies have begun to determine markers that are associated with progression in different breast cancer subtypes (2-17). Relevant models that recapitulate the morphological and molecular aspects of progression within subtypes are needed to determine which of these molecular changes function in acquisition of the invasive phenotype.

Culture models of human breast cells could provide such an opportunity if relevance to cancer progression *in vivo* were established. Pathways associated with transition to malignancy have traditionally been studied using either transgenic mouse models or primary human cells *engineered* to express genes with oncogenic properties. To deal with the heterogeneity of human breast tumors, cell lines originating from a large number of malignant breast carcinomas have been employed (18). It would be useful also to have models of 'spontaneous' transition to malignancy -as opposed to transgenic- which could include intermediate non-invasive and pre-invasive stages of carcinogenesis -as opposed to modeling only the invasive carcinoma stage. Such models could facilitate the discovery of steps in progression to the invasive phenotype in a context which recapitulates more of the complexity of carcinogenesis.

The HMT-3522 human breast epithelial cell line series (S1, S2, and T4-2) were derived from a reduction mammoplasty specimen of a patient with fibrocystic breast disease more than 20 years ago. The epithelial component of the tissue was grown in defined medium to give rise to S1 cells that became immortalized spontaneously; these cells are EGF-dependent for growth and are non-tumorigenic (19). Continuous culturing in the *absence* of EGF gave rise to a cell population referred to as S2, a cell line that is heterogeneous and essentially still non-malignant (20). Frequent inoculation of S2 cells into mice eventually produced a rare tumor which was cultured and passaged again through mice (20). The cell line derived from this tumor is referred to as T4-2 (20). Previously, we designed a three dimensional laminin-rich basement membrane (3DlrBM) assay to model both the normal breast and breast cancers (21) (Figure 1A). In 3DlrBM, S1 cells produce growth-arrested acini that express differentiation markers mimicking *in vivo* polar patterns of localization of a number of markers (21): S2 colonies are heterogeneous (this report), and T4-2 cells form large and disorganized colonies (22).

Here, we isolated three essentially homogeneous cell populations from S2 cells which we refer to as S3-A, S3-B, and S3-C using colony size in 3DlrBM as a screening tool (Figure 1A). These cells were non-invasive but had a higher potential for acquiring invasiveness than the parent S2. We found a substantial number of similarities between the model of S3 vs. T4-2 and pre-invasive to invasive transition in breast carcinogenesis based on progressive loss of tissue polarity, ability to form tumors with squamous and basal metaplastic histology, 76% similarity to recurrent CGH abnormalities found in breast tumors, and gene expression changes in classes of genes previously identified as being important for malignancy and invasion. These observations establish the S3 cell lines as the pre-invasive counterpart of a model of breast cancer progression within a *metaplastic context*. Using matrix metalloproteinases we demonstrate the utility of this model in identifying functionally significant changes in transition from the pre-invasive to the invasive phenotype in metaplastic breast cancer. The usefulness of the model is demonstrated further in another report (23) which describes the discovery of a novel pathway involved in invasion using this progression series.

Materials and Methods

Cell culture. S1 and T4-2 cells were grown in tissue culture monolayers (2D) using Falcon^{TM} tissue culture plastic or 3D in lrBM (Matrigel^{TM}) in defined medium as described previously(21, 22), S2 and S3 cells were grown under the same conditions as T4-2.

Indirect immunofluorescence analysis and image acquisition in 3DlrBM. Cells in 3DlrBM were embedded in sucrose and frozen on dry ice in Tissue-Tek OCT (Miles Laboratories), sectioned and immunostained as described previously (22).

Comparative Genomic Hybridization (CGH). Chromosomal CGH and BAC array CGH were performed essentially as described previously (24). Hierarchical clustering analysis was performed with GeneSpring software (Silicon Genetics), using standard correlation with a minimum distance metric of 0.001 to determine relatedness of cell lines. This was done using both the chromosomal and the BAC array data, with only significant amplification/deletion data points, as well as with the complete datasets, producing comparable results.

Analysis of tumor formation *in vivo*. We injected the cells into female balb/c athymic nude mice (Simonsen laboratories), measured tumors weekly using a calipher, and graphed the tumor frequency and volumes of tumors taken out after 9-10 weeks of tumor growth at which time the animals were sacrificed.

Statistical analysis of the mean tumor volumes was performed by pair-wise comparison using one-tailed homoscedastic t-test analysis. We injected 10 million cells subcutaneously into the rear flanks, or 5 million cells in 50% Matrigel^{TM} subcutaneously into the front flanks, or 2 million cells into the left and right fourth inguinal mammary glands. Tumors from all injections and surrounding tissues were fixed in 4% formaldehyde, paraffin embedded, sectioned into 5μm slices, and stained with Hematoxylin and Eosin –H&E (HRL laboratories, Hercules, CA). 350 H&E sections were examined independently by two expert breast pathologists (ADB and RAJ).

Global mRNA expression analysis by cDNA microarrays. cDNA microarrays with ~8000 known gene spots on poly-L-lysine-coated chips (custom arrayed at LBNL using Research Genetics 8k human clones) were used. mRNA samples were directly compared to each other by co-hybridization to the same slide using dendrimer technology to label with red-Cy5 or green-Cy3 (Genisphere). Total RNA (1μg) isolated with Qiagen RNEasy reagents was used for each sample hybridized. Cells in 3DlrBM were extracted using 5mM EDTA in cold PBS to dissolve the Matrigel™. For each comparison, 3 independent sets of cultures were processed, and cells were examined at day 10 of culture. For each comparison, 4 slides were hybridized. This corresponded to 3 sets of RNAs from independent cultures plus a dye-swap experiment in which the red and green label was switched for the two samples in question. Data were analyzed as described in SF 8.

RT-PCR. 1-Quantitative. The RNA prepared for microarrays was used to prepare cDNA after DNAse I (Invitrogen) treatment, using Superscript First-Strand Synthesis System for RT-PCR (Invitrogen). Quantitative real time PCR was done using Lightcycler (Roche) and FastStart SYBR Green (Roche). Primer sequences were as follows (5' -to- 3'): MMP13 forward aagatgcatccaggggtcct, MMP13 reverse gtccaggtttcatcatcatca; GAPDH forward cccctggccaaggtcatccatgac, GAPDH reverse cataccaggaaatgagcttgacaaag. Lightcycler reaction cycles were as recommended by Roche with the following modifications: For MMP13, 57°C for annealing, 27 seconds of extension, and signal acquisition at 84°C; for GAPDH, 56°C for annealing and 25 seconds for extension. 2-Semi-quantitative RT-PCR for MMP9, MMP13, MMP15, and MMP17 was performed using the following primer sets (5'-to-3'): MMP9 (forward: atgcgtggagagtcgaaatc, reverse: tacacgcgagtgaaggtgag), MMP13 (forward: aagatgcatccaggggtcct, reverse: gtccaggtttcatcatcatca), MMP15 (forward: ccatatgtccaccatgcgtt, reverse: atgatggcattggggttgct), MMP17 (forward: acgcaagaggagctgtctaag, reverse: acatggcttaacccaatggc), and conditions (after having determined linear range): MMP9, MMP15, and MMP17 (96°C 3min, 34x[96°C 30sec, 55°C 1min, 72°C 1min], 72°C 5min), MMP13 (96°C 3min, 29x[96°C 30sec, 55°C 30sec, 72°C 1min] 72°C 5min).

Expression analysis of cell surface proteins by FACS. Live cells were immunostained in suspension prior to fixing with 2% paraformaldehyde. Primary antibodies were used at 1:10 dilution, and FITC-conjugated secondary antibodies were used at 1:100 dilution. Primary antibodies were: MMP15, clone 162-22G5 (Oncogene); MMP17, rabbit polyclonal 475934 (Calbiochem). FACS analysis was performed using EPICS XL-MCL data acquisition and display software on XL flow cytometry analyzers (UC Berkeley, Flow Cytometry Facility). Gating of FLS (Forward Light Scatter) vs. LS (90 degree scatter) allowed us to obtain data relevant to intact cells only, FITC fluorescence peak was evaluated for its median value and was corrected using samples that had not been treated with primary antibody.

Gelatin zymography. Conditioned medium (for 48 hrs) from 10 day cultures of S1, S2, S3, and T4-2 were used. Samples were analyzed by SDS-PAGE zymography (25) to determine the molecular weights and the relative abundance of the gelatinases present.

Invasion assay. The ability to invade through lrBM (Matrigel™) was measured in Boyden chamber assays, essentially as described (26). The number of invading T4-2 or S3-C cells (out of 1 X 10^5 seeded) was determined after 48 hrs of incubation in either regular growth medium, in medium containing T4-2 conditioned medium (CM), in medium with DMSO, with different concentrations of the MMP inhibitor, GM6001 (AMS Scientific), or its inactive analog (C1004), or with CM that had previously been treated with DMSO, GM6001, or C1004. For siRNA treated T4-2 cells, transfection of 30-to-150nM oligo with 4μl of siPORT NeoFX (Ambion) per ml of media was performed 1 day after plating cells at regular density. siRNAs were allowed to down regulate protein levels for 2 days. Cells were then trypsinized and 1x10^5 cells were seeded for Boyden chamber assays. siRNAs against MMP9 (oligo 1: Ambion ID143941; oligo 2: Ambion ID 113182: oligo 3: Ambion ID 113183), MMP13 (oligo 1: Ambion ID 143556; oligo 2: Ambion ID 212725; oligo 3:Ambion ID 112915), MMP15 (oligo 1: Ambion ID 112917; oligo 2: Ambion ID 143557; oligo 3: Ambion ID 112916) MMP17 (oligo 1: Ambion ID 105396; oligo 2: Ambion ID 113514; oligo 3: Ambion ID 24016), or scrambled control siRNA (Ambion, Silencer™-Cy3 labeled) were used.

Immunohistochemistry. <u>Ki67.</u> Formalin fixed mouse xenograft tissue was paraffin embedded and sectioned into 5 μm thick tissue sections (HRL laboratories, Hercules, CA). The paraffin was removed by serial incubation in Xylene, 100% ethanol, 95% ethanol, 70% ethanol, and water. Tissues were blocked in 3% hydrogen peroxide in PBS for 5 minutes. Antigen retrieval was performed by incubating in 0.01% pre-warmed trypsin in PBS for 15min, followed by 10 minutes of microwaving in 10mM sodium citrate

buffer. Tissues were blocked in 1.5% normal horse serum in PBS for 30 minutes and incubated with primary Ki67 antibody which specifically recognizes human but not mouse Ki67 protein (Calbiochem, Anti-Ki-67-Human (Mouse), NA59) at 5μg/ml overnight at 4°C. Slides were washed with PBS and incubated with biotinylated anti-rabbit antibody (1:200 dilution, Vector Laboratories, Biotinylated anti-mouse IgG / anti-rabbit IgG (H+L), BA-1400) for 30 minutes at room temperature, followed by streptavidin-HRP (Vector Laboratories, Vectastain ABC kit, Elite PK-6100) for 30 minutes, and complete DAB (3,3'-Diaminobenzidine tetrahydrochloride, SIGMA) medium for 5 minutes. Slides were washed and counterstained with hematoxylin, followed by dehydration in 70% ethanol, 95% ethanol, 100% ethanol, Xylene, and coverslips mounted using Permount (Fisher Scientific, SP15). Strong nuclear staining was scored as positive and %Ki67 positive nuclei were determined for at least three tumor areas for each cell type injection, counting a minimum of 100 cells per area. **p63**. Immunohistochemistry was performed essentially as described for Ki67, except for omitting the trypsin step in antigen retrieval and increasing hydrogen peroxide blocking to 15 minutes. Primary antibody (Lab Vision, p63 Ab-1 clone 4A4) was used at 2μg/ml. **CK5/6, ER, PR**. Immunohistochemistry was performed as described in (27) using CK5/6 primary antibodies from Zymed (1:100), ER from DAKO (1:25) and PR from DAKO (1:200) and for **HER2-neu**, the Herceptest kit from DAKO was used.

Results

S3 cells display partial loss of tissue polarity in 3DlrBM, and a pre-invasive phenotype
Using colony size in 3DlrBM as an initial screen, we isolated multiple small, medium, and large sized colonies, expanded and propagated these clones for at least six generations, and examined their morphology in the 3D assay (Figure 1B). We chose three isolates that essentially bred true for the size of colony formed. We refer to these as S3-A, S3-B, and S3-C cell lines where colony size is A<B<C. S3-A cultures contain ~10% very large colonies (not shown); otherwise the colony size, especially for S3-C's, is essentially homogeneous. S3 cells displayed intermediate phenotypes compared to S1 and T4-2 colonies in 3DlrBM, as determined by markers that have been used extensively to describe tissue (acinar) polarity (22, 28-31) such as basolateral expression of β catenin, basal β4 integrin, cortical actin, and Ki67 labeling (Figure 1C). In Boyden Chamber assays S1, S2, and S3 cell lines did not invade lrBM but T4-2 cells were invasive (Figure 1D). When conditioned-medium (CM) from T4-2 cells was added to the chambers, S1 and S2 cells, they did not invade whereas S3-A, S3-B, and S3-C became invasive with the S3-C cells displaying the highest propensity to invade: T4-2>C>B>A.

S3 cells display an intermediate potential to form tumors.

We determined tumorigenicity of the cells when injected into nude mice under three different microenvironments: in the flank with cells alone or cells plus Matrigel, and into mammary fat pads with cells alone (Figure 2). In none of the injections did S1 cells or media control produced any measurable growth but T4-2 cells formed palpable tumors at high frequency as shown also previously (20, 22, 32, 33) (Figure 2A-C, top panel) When injected subcutaneously, S2 cells and the S3-series formed very small tumors at low frequencies. Subcutaneous injection in the presence of Matrigel (Figure 2A-C, middle panel) resulted in tumor formation in 50% of S2, 75% of S3-A, 73% of S3-B, 56% of S3-C (please see the section on tumor histology, below), and 100% of T4-2 cell injection sites. Importantly, mammary fat pad injections (Figure 2A-C, bottom panel) resulted in progressively increasing tumor frequency going from S2, S3-A, S3-B, S3-C, to T4-2 mirroring the rate of invasion observed in Boyden chambers (Figure 1D). Comparing the p-values for tumor volume (Figure 2C) showed that the mammary fat pad most clearly distinguished the non-tumorigenic S1, pre-invasive S3, and the malignant T4-2.

Tumor histology reveals similarities to cancer progression within a metaplastic context. In subcutaneous injections (SF 1B), the T4-2 tumors had viable, dividing cells with squamous metaplastic morphology. The S2 and S3 tumors had non-dividing cells suggesting they did not maintain growth, but they contained keratin clusters and inflammatory cells which are characteristics of well-differentiated squamous carcinomas of the breast. An average increase of 27 fold in tumor volume was observed when half the number of cells was injected in the presence of Matrigel (lrBM). In the Matrigel injections (Figure 2A-D middle panel, Supplemental File: SF 1A,C), 5/18 of the S1 injection sites showed a phenotype similar to low grade adenosquamous carcinomas despite the lack of a palpable tumor at the time of sacrifice (Figure 2J). Whereas 100% of the S2 and S3 tumors displayed the more benign mixed tumor histology, only 25% of the T4-2 tumors were mixed with the remainder being pure squamous. In addition, T4-2 tumors had features of higher grade squamous carcinoma than did the S2 and S3 tumors: 83% of the S2 and S3 tumors were well-differentiated compared to only 11% of the T4-2 tumors. Soft tissue involvement indicating either invasion or proliferative expansion into neighboring tissues was observed only in T4-2 tumors (Figure 2J). Similarly, calcifications which are an indication of necrosis usually observed in high grade tumors were found in almost all T4-2 tumors but only in a few of S2 or S3s. The fat pad tumor histology also showed similarities to squamous metaplasias of the breast (Figure 2J, SF 1D) with T4-2 tumors being higher grade in general, based on the degree of differentiation, soft tissue involvement, and calcification phenotypes.

S3 cells display genomic aberrations that are distinct from those found in S1 and T4-2, but are relevant to some human breast cancers. We determined the genomically amplified or deleted regions by comparative genomic hybridization (CGH) (SF 2). The number of aberrations increased progressively when S1, S2-S3 and T4-2 cells were compared (Figure 3A-B). Hierarchical clustering analysis (Figure 3C) showed that the S2-S3 and T4-2 cell lines were more closely related to each other than they were to the S1 cells, and that the malignant T4-2 chromosomal aberration profiles were distinct from those of the S2-S3 cells. S2, S3, T4-2 cell lines contained 76% (22 of 29) of the chromosomal gains or losses that are reported to be commonly found in primary breast tumors (Figure 3D). Of the aberrations recurrently found in carcinoma in situ (pre-invasive), 6/10 were present in S3-A, S3-B, and S3-C cells; but all 10 were found in T4-2. The aberrations that were present in T4-2 but not in S3 were those found in high grade in situ or invasive carcinomas.

Transition from S3-C to T4-2 phenotype is associated with altered expression of gene classes previously implicated in human breast cancer progression. We determined differences in global gene expression between S3-C and T4-2 when cells were grown either in 2D (monolayers) or in 3DlrBM cultures (SF 3). To discover groups of genes with shared attributes in an unbiased manner, we analyzed these two sets of differentially expressed genes by model-based clustering according to their Gene Ontology (GO) terms and other annotations by developing and using a method called Attribute Profile Clustering (34) (SF 8). The 141 genes altered between S3-C and T4-2 in 2D were placed into four groups summarized as integral membrane proteins, transcription factors, kinases, and transport molecules (SF 4, 6, 8). The groups for the 502 genes with different expression between S3-C and T4-2 when grown in 3D were integral membrane proteins, transcription factors, kinases, and chemokines (SF 5,7, 8). The best defined group in the comparison of S3-C and T4-2 in 3D, but not 2D, revealed a class with 100% of the genes sharing the GO term "Chemokine Activity". Chemokines have previously been shown to play a significant role in metastasis (35) and have been found in association with human breast cancer progression in patient tissues (36).

MMP9, 13, 15, and 17 are functionally significant in the acquisition of invasiveness. In addition to the genes that were relevant to human breast cancer progression by attribute clustering analysis, the microarray data contained another class of genes, the matrix metalloproteinases (MMPs), that demonstrated differential expression when S3-C and T4-2 were compared only in 3DlrBM. Microarray analysis showed that MMP13 (collagenase-3), MMP15 (MT-2 MMP), and MMP17 (MT-4 MMP) had approximately 30% higher expression in T4-2 versus S3-C in 3D cultures (SF 3). For MMP13, we confirmed these results using quantitative RT-PCR (Figure 4A) and western blots of CM (not shown). For

the membrane-bound MMP15 and MMP17, FACS analysis showed that cell surface expression was higher in T4-2 than in S3-C cells (Figure 4B-C). MMP15 has been shown to activate proMMP2 by cleavage (37). Therefore, we determined overall gelatinolytic activity, including MMP2 and MMP9 activity, present in S1, S2, S3, and T4-2 cell lines using zymograms. S1 cells expressed proMMP2 but not MMP9; S2, S3-A, S3-B had no detectable expression of MMP2 or MMP9; S3-C had a small amount of proMMP9 expression and T4-2 showed high levels of proMMP9 but no MMP2 expression (Figure 4D).

In this model, we could directly assess the significance of MMP expression changes for the invasive phenotype. A broad-spectrum MMP inhibitor, GM6001 (38), abrogated T4-2 invasiveness whereas treatment of cells with C1004 an inactive analog of GM6001, had no detectable effect (Figure 5B). To confirm the inhibitor data specifically, we used siRNAs to transiently and individually knock down the levels of MMP9, 13, 15, and 17 (Figure 5A) and found that siRNAs which successfully knocked down these MMPs decreased the amount of invasiveness of T4-2 cells compared to the scrambled control siRNA (Figure 5C). MMPs were important for acquisition of invasiveness in S3-C cells as well: addition of GM6001, and not the control C1004, to either the S3-C or T4-2 media (the CM was taken from the latter) inhibited the ability of the T4-2 CM to induce invasiveness in S3-C (Figure 5D).

Discussion

Modeling human breast cancer in culture traditionally has relied on carcinoma-derived cell lines or addition of potent oncogenic stimuli to non-malignant cells. What we have lacked so far are models with which we can recapitulate intermediate stages of cancer progression to simulate the complexity of different types of breast cancers (39). Here we describe one such human cell culture model. Neither the process of immortalization nor the process of selection of the pre-invasive S3 or malignant T4-2 cells entailed introduction of oncogenic transgenes. The model is not biased towards either one or more pathways but provides a transgene-free opportunity to study the involvement of different and possibly unrelated pathways in malignant transition (Table 1, SF 8). The cell lines produced tumors with various metaplastic features, such as rare low grade adenosquamous carcinoma, mixed benign tumors, and aggressive squamous metaplasia suggesting progression within a metaplastic context.

Pure squamous carcinomas of the breast are rare, although mixed adenocarcinomas are diagnosed at a higher frequency (40). Some studies describe squamous metaplastic breast cancers as being extremely

aggressive and they have been characterized to be at least as aggressive as grade 3 hormone receptor-negative adenocarcinomas (40-43). Five year survival for patients with pure squamous carcinomas of the breast appears to be only marginally worse than what is reported for all breast cancers, although these comparisons suffer from lack of a sufficient number of squamous carcinomas with follow up data (41). Squamous metaplasias of the breast share similarities with the aggressive basal-like subtype of carcinomas in clinical behavior as well as in the expression of a panel of markers (40, 44). HMT-3522 cells resemble the basal-like subtype of breast cancers at the molecular level by gene expression profiling (45). In addition, the HMT-3522 xenograft tumors are p63 and CK5/6 positive as well as being ER, PR, and HER2 negative (SF 1F-G), similar to myoepithelial/basal cells and squamous metaplastic carcinomas (46). In addition to the rare pure squamous carcinomas of the breast, 39% of breast cancers in pre-menopausal African-Americans and the majority of tumors in BRCA1 mutation carriers are ER-PR negative, and have basal characteristics (47, 48). Understanding whether such similarities in marker expression translate to overlap in the mechanism of transition to invasiveness would require developing models that recapitulate these subtypes, as described for at least one subtype developed here.

The HMT-3522 cells display xenograft tumor histology consistent with the breast cancer type represented by their molecular makeup. This is a rare situation. Most human breast cancer cell line xenografts display an undifferentiated phenotype (observations of ADB). To our knowledge, in addition to the cell line model described here, the MCF10A series of Ha-Ras transformed cell lines comprise the only other model which recapitulates some of the histological characteristics of human carcinomas (DCIS and IDC) as xenograft tumors (49). In order to capture a more complete picture of the malignant progression *in vivo*, more complex microenvironments need to be created in 3D cultures, and a number of laboratories including ours are engaged in this endeavor.

Comparison of the phenotypes of S3 cells in culture to their ability to form tumors in three different microenvironments *in vivo* show that these cells are particularly sensitive to their host microenvironment producing complex phenotypes *in vivo*. For example, the S3-A cell line throws off ~10% large colonies in the 3DlrBM but these do not invade through lrBM in Boyden chambers possibly because the duration of the assay is too short (two days). However, S3-A tumor frequency is higher than the other S3s in the skin injections -but interestingly not in the skin+Matrigel or fat pad injections- and the S3-A tumor volumes in the skin+Matrigel and fat pad injections are higher than the other S3s (Figure 2). The other S3 cell lines also appear to be very sensitive to their particular host microenvironment, resulting in the breakdown of a one-to-one correlation between the progressive phenotypes observed in culture for S3-A, S3-B, and S3-C and the more complex phenotypes found in the xenografts. It is conceivable that, given the length of the

9-10 week period of time, the host microenvironment within which the injected cells are in dynamic and reciprocal interactions with the stromal and humoral factors could allow for selection of the aggressive subpopulations, resulting in gain or loss of necessary functions to become malignant. In addition, results confirm that the cells poised to become malignant have not yet inactivated all pathways or gained all the new functions needed for a stable malignant phenotype.

What was found to be consistent across all assays performed (invasion, 3D polarity, CGH profile, tumorigenicity) is that all of the S3 cells displayed a phenotype *distinct* from both S1 and T4-2 cells *in vivo* as well as in the 3DlrBM assay. For tumorigenicity, this was supported by statistical analysis of tumor volume, as well as by histological analysis showing that S3 tumors manifested more benign characteristics than the T4-2 tumors. Also, the S3 cells displayed more homogeneous phenotypes and a higher propensity to become invasive than the parent S2 cells when induced with T4-2 conditioned-medium. Therefore by these criteria, S3 cells have indeed *progressed* further than their parent S2 cells towards malignancy, and are *intermediate* between the non-tumorigenic S1 and malignant T4-2s.

Here we have described this model as one of transition from pre-invasive to invasive phenotype, to mimic the multi-step carcinogenesis hypothesis of breast cancer (50, 51). However, the emerging cancer stem/progenitor cell hypothesis also needs to be considered. Sontag and Axelrod have proposed four separate models to describe how atypical hyperplasia, ductal carcinoma in situ, invasive ductal carcinoma and metastasis may relate to each other (1). These are the linear, non-linear, branched, and parallel pathways. Unlike the other three hypotheses, the parallel pathway does not assume that in situ carcinoma develops into invasive carcinoma, but rather that in situ and invasive carcinomas can arise from the same progenitor. In our cell lines, S2 gave rise to both the pre-invasive S3-C and the invasive T4-2 cells via different steps of manipulation in culture and in mice, respectively (Figure 1A). Therefore, it is tempting to speculate that the model described here could be placed as supporting the parallel progression hypothesis. Regardless of which mathematical model we consider, what we have developed are human breast epithelial cells with pre-invasive and invasive characteristics which recapitulate some aspects of pre-invasive and invasive carcinomas with basal and squamous histologic and molecular phenotypes.

Analysis of this malignant transition in 3D cultures allowed us to identify candidate genes as potential therapeutic targets. For example, of the MMPs we identified as having a function in invasion- MMP9, MMP13, and recently MMP17 have been shown to be associated with- and increased in- breast cancer progression (52-54). Although broad spectrum inhibitors of MMPs have failed in clinical trials, targeting specific genes for certain subtypes of cancers may eliminate non-specific effects, thereby producing more

desirable clinical outcomes (55). In addition to the list of genes differentially expressed between S3-C and T4-2 (Table 1, SF 8), this model system is conducive to functional siRNA screens probing either gain of invasion function in S3-C or loss of invasion of T4-2 to find new genes involved in invasion. Using the same model, we recently discovered a new pathway of invasion regulated by polo-like kinase I (23). In general, the results described here provide a proof-of-principle for the development of *spontaneous* transition models for additional subtypes of breast cancers, with potential utility in discovering other mechanisms of invasion and other potential targets for therapy

Acknowledgements

Figure Legends

Figure 1. Partial loss of tissue polarity, and pre-invasive phenotypes of S3 cells
A. Steps involved in the isolation of the HMT-3522 series of cell lines. **B.** 3DlrBM cultures of HMT-3522-S2 cells and small (S3-A), medium (S3-B) and large (S3-C) colonies isolated from the parent culture of S2, on day 10. **C.** Confocal images of immunostained colonies in 3DlrBM, day 10. **D.** Invasion assays: two experiments, triplicate samples. Black bars, untreated cells; gray bars, cells treated with T4-2 conditioned medium (CM).

Figure 2. S3 cells display low tumorigenicity and squamous metaplastic phenotype in nude mice

A. % injection sites that produced tumors sustained for the duration of the experiment; **top:** *Subcutaneous injections:* Three experiments; 14 S1, 22 S2, 20 S3-A, 16 S3-B, 22 S3-C, 30 T4-2, and 3 media controls; **middle:** *Subcutaneous + Matrigel injections:* Two experiments; 18 S1, 18 S2, 20 S3-A, 22 S3-B, 18 S3-C, and 18 T4-2 injections. **bottom:** *Mammary fat pad injections:* 15 S1, 16 S2, 16 S3-A, 16 S3-B, 15 S3-C, 24 T4-2, and 4 media controls. **B.** Mean tumor volume (in mm^3) excised from sacrificed animals; **C.** p-values for the volume comparisons indicated; p<0.05 in bold; **top:** *Subcutaneous injections*, **middle:** *Subcutaneous + Matrigel injections*, **bottom:** *Mammary fat pad injections*. **D**. H&E images of S1, S2, S3-B subcutaneous + Matrigel tumors, and S3-A, S3-C, T4-2 fat pad tumors; scale bar 50 μm. **S1**, low grade adenosquamous carcinoma-like phenotype at the injection site; **S2**, squamous differentiation with whorls and bridges, transition from cuboidal cells to larger squamous cells in the center; **S3-A**, well-differentiated area with a small cyst, less well differentiated area with calcification; **S3-B**, cords of cells surrounding areas of extracellular matrix showing solid tumor areas with proliferation and squamous differentiation and displaying pleomorphic adenoma phenotype, **S3-C**, squamous differentiation, foamy squamous carcinoma cells, abundant stromal reaction; **T4-2**, squamous carcinoma invading the skeletal muscle.

Figure 3. CGH profile of S3 cells compared to other HMT-3522 cells and to primary tumors
A. Chromosomal amplifications (red) and deletions (green) for each cell type examined at the indicated passage number (e.g. S1_27 = S1 cells at passage 27). **B.** Chromosomal aberrations common to all cell lines shown on the left, e.g. "S1" means, common to all S1 lineages shown in part A. **C.** Hierarchical clustering of 119 significantly amplified or deleted regions for the indicated cell lines. **D.** Chromosomal aberrations commonly found in primary tumors, as described in each study cited; shown in bold if shared with HMT-3522 cell lines; complete list of aberrations shared between the cell lines and primary tumors listed at the bottom (TOTAL).

Figure 4. Candidate MMPs from microarrays are differentially expressed between S3-C and T4-2 cells
A. Quantitative RT-PCR for MMP13 normalized to GAPDH internal control, for S3-C and T4-2 in 3DlrBM; p-value <0.05. **B-C.** Cell surface expression of MMP15 and MMP17: four independent experiments; p-value < 0.05. **D.** Zymogram detecting gelatinoylitic activity in cell lines, compared to APMA (p-Aminophenylmercuric Acetate)-activated recombinant MMP2 control.

Figure 5. Candidate MMPs function in invasion through lrBM

A. RT-PCR for MMP9, 13, 15, and 17 in cells transfected with siRNAs to the respective MMPs or a scrambled control (Scr.). **B.** Invasion assays for T4-2 cells treated with the indicated MMP-inhibitor or control: two experiments, duplicate samples. **C.** Invasion assays for T4-2 cells transfected with MMP9, 13, 15, or 17 siRNAs vs. Scr.; p-values compared to Scr. **D.** Invasion assays for S3-C cells, number of invading cells normalized to S3-C cells treated with T4-2 CM ; "post-treated": CM was added to the S3-C medium after the indicated MMP-inhibitor or control (40μm), "pre-treated": CM was pre-treated with the MMP-inhibitor or control (40μm) for 48 hrs before being added to the S3-C medium in the invasion assays: three experiments.

Table 1. Attribute profile clustering of differentially expressed genes between S3-C and T4-2
The titles (e.g., Transport, Kinase, etc) describe the most common gene function in each class; the ratio of genes in the class that fit this functional definition is shown in parenthesis. For each gene, the row of information contains a Genbank number (e.g., NM_005050), a gene name (e.g. ABCD4), the mean value of the ratio of T4-2 / S3-C expression over 4-microrarray experiments (e.g. 0.15), and t-test, penalized p-value, $p < 0.05$

Supplemental Files (SFs)
SF 1. Xenograft tumors. A. Ki67 staining of tissue sections obtained from tumors formed by injection of S3-A, S3-B, S3-C, and T4-2 cells with lrBM. Positive and negative nuclei are shown with arrows. The diffuse non-cellular staining in tumors is the injected lrBM. Graph shows % Ki67 staining for S3-A, S3-B, S3-C, and T4-2 xenograft tumors (with lrBM). At least three tumor areas were counted to determine mean and standard error. **B.** Subcutaneous xenograft morphology. An S3-A tumor area (top panel), showing keratin pearls, massive infiltration, and non-dividing squamous epithelial cells; a low and high magnification photomicrograph of a T4-2 tumor (middle and bottom panels), showing actively dividing squamous breast epithelial cells within the subcutaneous tumor. **C.** Matrigel-induced pleomorphic histology in the subcutaneous tumor. An S3-A tumor (left panel), showing extensive matrix deposition, basal epithelial, and squamous epithelial cells; a T4-2 tumor (right panel), containing mostly squamous carcinoma cells. **D.** Fat pad xenograft morphology. A small, well differentiated S3-C tumor with few foamy squamous cell carcinoma cells; a T4-2 tumor; local high grade with local inflammation; calcifications. **E.** S3-A tumor containing excessive cystic area. A large cyst encompassing most of the volume of an S3-A tumor of cells injected subcutaneously with Matrigel. **F.** Nuclear p63 immunohistochemical signal (brown) in a T4-2 tumor grown in the fat pad displaying a diffuse pattern characteristic of squamous cell carcinomas. **G.** ER, PR, HER2, and CK5/6 immnohistochemistry in T4-2 tumors of cells injected subcutaneously with Matrigel, showing triple receptor negative and CK5/6

positive phenotype. ER and PR control are receptor-positive IDC, CK5/6 control is tonsil tissue with positive histiocytes and negative lymphocytes.

SF 2. CGH data. *Chromosomal CGH Results.* 1200 data points per chromosome represented as normalized log2 values. First raw shows cell type and passage number, first column lists chromosome number/name. *Chromosomal Summary:* List of gains and losses per cell line and passage listed in the first column. *Chromosomal Cytobands:*Estimated cytobands involved in each amplification and deletion determined by chromosomal CGH analysis. *BAC Array CGH Results.* Spot # column shows unique location on the array, Gene/Locus column lists the BAC name which can be found on the 950_BAC information worksheet in order to link to the UCSC database and find which genes are on each BAC, Loc. column lists the genomic cytoband location, remaining columns list the normalized log2 values for each BAC spot, for the indicated cell line and passage. Red indicates significant deletions, green indicates significant amplifications. *950_BAC information* and *Extra BAC Info* contain links to the UCSC genome browser for determining details about each BAC clone.

SF 3. Global gene expression data. Worksheet titles containing "All genes" show gene expression differences between either S1 and T4-2 or S3-C and T4-2 for all ~8000 genes on the arrays. The normalized ratios represent T4-2/S3-C or T4-2/S1. Worksheet titles containing "Differential" show gene expression differences that have a penalized p-value of 0.05 or lower. *S1-T4 (or S3-T4) CGH-Expression* lists all BAC clones with potential to produce gene expression differences between the two cell lines compared. All genes present on each BAC clone are listed. Of these, the ones present on the cDNA expression arrays are in bold. For these genes, expression differences (normalized mean and p-values) between the two cell lines (compared in 2D or in 3D) are shown. Gene expression patterns that correspond to expected patterns from CGH analysis are in bold.

SF 4. and 5. Attribute clustering results. Gene clusters for the differentially-expressed genes between S3-C and T4-2 in 2D (4), and S3-C and T4-2 in 3D (5).

SF 6. and 7. Influential attributes. List of influential attributes for each cluster, as well as the summary, for attribute clustering results for differentially expressed genes between S3-C and T4-2 in 2D (6), or in 3D (7).

SF 8. Experimental procedures supplement. Detailed descriptions of how the gene expression data was analyzed and how attribute profile clustering was performed.

References

1.   Sontag L, Axelrod DE. Evaluation of pathways for progression of heterogeneous breast tumors. J Theor Biol 2005;232:179-89.

2.   Buerger H, Otterbach F, Simon R, et al. Comparative genomic hybridization of ductal carcinoma in situ of the breast-evidence of multiple genetic pathways. J Pathol 1999;187:396-402.

3.   Etzell JE, Devries S, Chew K, et al. Loss of chromosome 16q in lobular carcinoma in situ. Hum Pathol 2001;32:292-6.

4.   Gong G, DeVries S, Chew KL, Cha I, Ljung BM, Waldman FM. Genetic changes in paired atypical and usual ductal hyperplasia of the breast by comparative genomic hybridization. Clin Cancer Res 2001;7:2410-4.

5.   Isola J, Chu L, DeVries S, et al. Genetic alterations in ERBB2-amplified breast carcinomas. Clin Cancer Res 1999;5:4140-5.

6.   Isola JJ, Kallioniemi OP, Chu LW, et al. Genetic aberrations detected by comparative genomic hybridization predict outcome in node-negative breast cancer. Am J Pathol 1995;147:905-11.

7.   Loveday RL, Greenman J, Simcox DL, et al. Genetic changes in breast cancer detected by comparative genomic hybridisation. Int J Cancer 2000;86:494-500.

8.   Ma XJ, Salunga R, Tuggle JT, et al. Gene expression profiles of human breast cancer progression. Proc Natl Acad Sci U S A 2003;100:5974-9.

9.   Nishizaki T, DeVries S, Chew K, et al. Genetic alterations in primary breast cancers and their metastases: direct comparison using modified comparative genomic hybridization. Genes Chromosomes Cancer 1997;19:267-72.

10.   Nishizaki T, Chew K, Chu L, et al. Genetic alterations in lobular breast cancer by comparative genomic hybridization. Int J Cancer 1997;74:513-7.

11.   Polyak K. Molecular alterations in ductal carcinoma in situ of the breast. Curr Opin Oncol 2002;14:92-6.

12.   Porter DA, Krop IE, Nasser S, et al. A SAGE (serial analysis of gene expression) view of breast tumor progression. Cancer Res 2001;61:5697-702.

13.   Sgroi DC, Teng S, Robinson G, LeVangie R, Hudson JR, Jr., Elkahloun AG. In vivo gene expression profile analysis of human breast cancer progression. Cancer Res 1999;59:5656-61.

14.   Thor AD, Eng C, Devries S, et al. Invasive micropapillary carcinoma of the breast is associated with chromosome 8 abnormalities detected by comparative genomic hybridization. Hum Pathol 2002;33:628-31.

15.   Tirkkonen M, Tanner M, Karhu R, Kallioniemi A, Isola J, Kallioniemi OP. Molecular cytogenetics of primary breast cancer by CGH. Genes Chromosomes Cancer 1998;21:177-84.

16.   Waldman FM, DeVries S, Chew KL, Moore DH, 2nd, Kerlikowske K, Ljung BM. Chromosomal alterations in ductal carcinomas in situ and their in situ recurrences. J Natl Cancer Inst 2000;92:313-20.

17.   Waldman FM, Hwang ES, Etzell J, et al. Genomic alterations in tubular breast carcinomas. Hum Pathol 2001;32:222-6.

18.   Neve RM, Chin K, Fridlyand J, et al. A collection of breast cancer cell lines for the study of functionally distinct cancer subtypes. Cancer Cell 2006;10:515-27.

19.   Briand P, Petersen OW, Van Deurs B. A new diploid nontumorigenic human breast epithelial cell line isolated and propagated in chemically defined medium. In Vitro Cell Dev Biol 1987;23:181-8.

20.   Briand P, Nielsen KV, Madsen MW, Petersen OW. Trisomy 7p and malignant transformation of human breast epithelial cells following epidermal growth factor withdrawal. Cancer Res 1996;56:2039-44.

21.   Petersen OW, Ronnov-Jessen L, Howlett AR, Bissell MJ. Interaction with basement membrane serves to rapidly distinguish growth and differentiation pattern of normal and malignant human breast epithelial cells. Proc Natl Acad Sci U S A 1992;89:9064-8.

22.   Weaver VM, Petersen OW, Wang F, et al. Reversion of the malignant phenotype of human breast cells in three-dimensional culture and in vivo by integrin blocking antibodies. J Cell Biol 1997;137:231-45.

23.   Rizki A, Mott JD, Bissell MJ. Polo-like kinase I is involved in invasion through extracellular matrix. Cancer Research 2007;In press.

24.   Pinkel D, Segraves R, Sudar D, et al. High resolution analysis of DNA copy number variation using comparative genomic hybridization to microarrays. Nat Genet 1998;20:207-11.

25.   Herron GS, Werb Z, Dwyer K, Banda MJ. Secretion of metalloproteinases by stimulated capillary endothelial cells. I. Production of procollagenase and prostromelysin exceeds expression of proteolytic activity. J Biol Chem 1986;261:2810-3.

26.   Lochter A, Srebrow A, Sympson CJ, Terracio N, Werb Z, Bissell MJ. Misregulation of stromelysin-1 expression in mouse mammary tumor cells accompanies acquisition of stromelysin-1-dependent invasive properties. J Biol Chem 1997;272:5007-15.

27.   Taylor MA, Cote RJ. Immunomicroscopy: A Diagnostic Tool for the Surgical Pathologist. In: Saunders WB, editor.; 1994. p. 300-78.

28.   Liu H, Radisky DC, Wang F, Bissell MJ. Polarity and proliferation are controlled by distinct signaling pathways downstream of PI3-kinase in breast epithelial tumor cells. J Cell Biol 2004;164:603-12.

29.   Muthuswamy SK, Li D, Lelievre S, Bissell MJ, Brugge JS. ErbB2, but not ErbB1, reinitiates proliferation and induces luminal repopulation in epithelial acini. Nat Cell Biol 2001;3:785-92.

30.   Weaver VM, Lelievre S, Lakins JN, et al. beta4 integrin-dependent formation of polarized three-dimensional architecture confers resistance to apoptosis in normal and malignant mammary epithelium. Cancer Cell 2002;2:205-16.

31.   Lelievre SA, Weaver VM, Nickerson JA, et al. Tissue phenotype depends on reciprocal interactions between the extracellular matrix and the structural organization of the nucleus. Proc Natl Acad Sci U S A 1998;95:14711-6.

32.   Muschler J, Levy D, Boudreau R, Henry M, Campbell K, Bissell MJ. A role for dystroglycan in epithelial polarization: loss of function in breast tumor cells. Cancer Res 2002;62:7102-9.

33.   Wang F, Weaver VM, Petersen OW, et al. Reciprocal interactions between beta1-integrin and epidermal growth factor receptor in three-dimensional basement membrane breast cultures: a different perspective in epithelial biology. Proc Natl Acad Sci U S A 1998;95:14821-6.

34.   Semeiks JR, Rizki A, Bissell MJ, Mian IS. Ensemble attribute profile clustering: discovering and characterizing groups of genes with similar patterns of biological features. BMC Bioinformatics 2006;7:147.

35.   Muller A, Homey B, Soto H, et al. Involvement of chemokine receptors in breast cancer metastasis. Nature 2001;410:50-6.

36.   Allinen M, Beroukhim R, Cai L, et al. Molecular characterization of the tumor microenvironment in breast cancer. Cancer Cell 2004;6:17-32.

37.   d'Ortho MP, Will H, Atkinson S, et al. Membrane-type matrix metalloproteinases 1 and 2 exhibit broad-spectrum proteolytic capacities comparable to many matrix metalloproteinases. Eur J Biochem 1997;250:751-7.

38.   Grobelny D, Poncz L, Galardy RE. Inhibition of human skin fibroblast collagenase, thermolysin, and Pseudomonas aeruginosa elastase by peptide hydroxamic acids. Biochemistry 1992;31:7152-4.

39.   Leaf C. Why we're losing the war on cancer (and how to win it). Fortune 2004;149:76-82, 4-6, 8 passim.

40.   Hennessy BT, Krishnamurthy S, Giordano S, et al. Squamous cell carcinoma of the breast. J Clin Oncol 2005;23:7827-35.

41.   Aparicio I, Martinez A, Hernandez G, Hardisson D, De Santiago J. Squamous cell carcinoma of the breast. Eur J Obstet Gynecol Reprod Biol 2007.

42.   Tse GM, Tan PH, Putti TC, Lui PC, Chaiwun B, Law BK. Metaplastic carcinoma of the breast: a clinico-pathological review. J Clin Pathol 2006.

43.   Behranwala KA, Nasiri N, Abdullah N, Trott PA, Gui GP. Squamous cell carcinoma of the breast: clinico-pathologic implications and outcome. Eur J Surg Oncol 2003;29:386-9.

44.   Reis-Filho JS, Milanezi F, Steele D, et al. Metaplastic breast carcinomas are basal-like tumours. Histopathology 2006;49:10-21.

45.   Kenny PA, Lee GY, Myers CA, et al. The morphologies of breast cancer cell lines in three-dimensional assays correlate with their profiles of gene expression. Molecular Oncology 2007;In press.

46.   Tse GM, Tan PH, Chaiwun B, et al. p63 is useful in the diagnosis of mammary metaplastic carcinomas. Pathology 2006;38:16-20.

47.   Carey LA, Perou CM, Livasy CA, et al. Race, breast cancer subtypes, and survival in the Carolina Breast Cancer Study. JAMA 2006;295:2492-502.

48.   Honrado E, Benitez J, Palacios J. Histopathology of BRCA1- and BRCA2-associated breast cancer. Crit Rev Oncol Hematol 2006;59:27-39.

49.   Santner SJ, Dawson PJ, Tait L, et al. Malignant MCF10CA1 cell lines derived from premalignant human breast epithelial MCF10AT cells. Breast Cancer Res Treat 2001;65:101-10.

50.   Allred DC, Mohsin SK. Biological features of premalignant disease in the human breast. J Mammary Gland Biol Neoplasia 2000;5:351-64.

51.   Burstein HJ, Polyak K, Wong JS, Lester SC, Kaelin CM. Ductal carcinoma in situ of the breast. N Engl J Med 2004;350:1430-41.

52.   Nielsen BS, Rank F, Lopez JM, et al. Collagenase-3 expression in breast myofibroblasts as a molecular marker of transition of ductal carcinoma in situ lesions to invasive ductal carcinomas. Cancer Res 2001;61:7091-100.

53.   Rha SY, Yang WI, Kim JH, et al. Different expression patterns of MMP-2 and MMP-9 in breast cancer. Oncol Rep 1998;5:875-9.

54.   Chabottaux V, Sounni NE, Pennington CJ, et al. Membrane-type 4 matrix metalloproteinase promotes breast cancer growth and metastases. Cancer Res 2006;66:5165-72.

55.   Fingleton B. Matrix metalloproteinases: roles in cancer and metastasis. Front Biosci 2006;11:479-91.

Figure 1.

A


```
┌──────────────┐                          ┌──────┐
│  REDUCTION   │  Spontaneous             │ T4-2 │
│ MAMMOPLASTY  │  immortalization   S1    └──────┘
│  EPITHELIUM  │ ──────────────→  Selection  S2  Mice 2x
│              │  Defined medium    -EGF
│              │     +EGF                  Selection 3D   S3
└──────────────┘
```

B

S2

S3-A   S3-B   S3-C

C

	S1	S3-A	S3-B	S3-C	T4-2
Actin					
β-cat					
β4 int					
DAPI					
Ki-67					
%	5.1	26	48	65	72

D

Avg # of invading cells

Not induced   Induced by T4-2 CM

S1 S2 S3-A S3-B S3-C T4-2   S1 S2 S3-A S3-B S3-C T4-2

Figure 2.

Figure 3.

A

S1_27	1p	**5q**	**8q**	12q	13q	6pq
S1_50	**5q**	**8q**	20q	1p	**6pq**	18q
S1_54	5p	**5q**	7q	**8q**	12p	16p	20q	6pq	18pq
S1_108	**5q**	**8q**	20q	1p	**6pq**	18q
S1_177	**5q**	**8q**	20q	1p	**6pq**	18pq
S2_218	**3q**	**5q**	**8q**	**14q**	16q	1p	4p	6pq	8q	9p	13q	18pq	20p
S2_229	**3q**	5p	**5q**	**8q**	12p	**14q**	19p	22q	Xq	4p	6pq	8q	9p	13q	18pq	20p
S3-A_5	**3q**	5p	**5q**	**8q**	**14q**	21q	Xq	4p	6pq	8q	13q	18pq	20p
S3-B_4	**3q**	5p	**5q**	**8q**	12p	**14q**	16q	19p	22q	Xq	4p	6pq	8q	9q	13q	18pq	19q	20p
S3-C_5	**3q**	5p	**5q**	**8q**	12p	**14q**	22q	4p	6p	8q	13q	18pq	20p
S3-C_6	2q	**3q**	**5q**	**8q**	9q	12p	**14q**	22q	Xq	4p	6pq	8q	9p	13q	18pq	20p
T4_25	**3q**	**5q**	7pq	**8q**	9q	10q	12p	12q	**13q**	**14q**	**16pq**	17pq	**19p**	20q	21q	22q	Xq	4pq	**5pq**	6pq	8q	**9p**	13q
T4_27	**3q**	**5q**	7p	**8q**	10p	12p	**13q**	**14q**	**16p**	17q	**19p**	22q	3p	4p	**5pq**	6pq	8q	**9p**	13q	18pq	20p	Xp
T4_29a	**3q**	**5q**	7p	**8q**	9q	10p	12p	**13q**	**14q**	**16p**	**19p**	21q	1p	3p	4p	**5pq**	6q	8p	8q	**9p**	13q	18pq	20p
T4_29b	**3q**	**5q**	7p	**8q**	9q	10p	**13q**	**14q**	**16p**	**19p**	22q	1p	3p	4p	**5pq**	6q	8q	**9p**	13q	18pq	Xq
T4_30	**3q**	**5q**	7p	**8q**	9q	12p	**13q**	**14q**	**16pq**	17q	**19p**	22q	3p	4p	**5pq**	6q	8q	**9p**	13q	18pq	20p	Xp

B

S1	**5q**	**8q**	6pq
S2-S3	**3q**	**5q**	**8q**	**14q**	4p	6p	8q	13q	18pq	20p
T4	**3q**	**5q**	**8q**	**13q**	**14q**	**16p**	**19p**	**5pq**	8q	**9p**	13q

C

(dendrogram) T4_44, T4_30, S3-C_5, S3-B_5, S3-A_5, S3-B_7, S3-C_10, S2_220, S1_59, S1_50, S1_27

Groups: **T4-2**, **S2-S3**, **S1**

D

Study Reference	Primary Tumor Type	Commonly Found Chromosomal Gains and Losses
Buerger et al, 1999	DCIS	gain: 1q, **11q**, **17q**, loss: 16q
Waldman et al, 2000	DCIS	gain: **17q**, loss: **8p**, **17p**
Moore et al, 1999	High grade DCIS	gain: 1q, 6p, **11q**, **12q**, **16p**, **20q**, loss: **6q**, **9p**, **13q**
Etzell et al, 2001	LCIS	gain: 1q, loss: **8p**, 12q, 16q, **17p**
Gong et al, 2001	ADH, UDH	loss: 16q, **17p**
Tirkkonen et al, 1998	Carcinoma	gain: 1q, **5p**, **8q**, **11q**, **16p**, **17q**, **19p**, **19q**, **20q**, loss: **6q**, **8p**, **9p**, 11q, **13q**, 16q, **17p**, **18q**, **Xq**
Loveday et al, 2000	Carcinoma	gain: **1p**, 4q, **5q**, 6q, **13q**, **5p**, loss: 16q
Isola et al, 1995	Node negative carcinoma (recurrence)	gain: **8q**, **20q**
Isola et al, 1999	ErbB2 amplified carcinoma	gain: 1q, **8q**, **20q**, loss: **3p**, **13q**, **18q**
Nishizaki et al, 1997	Lobular carcinoma	gain: 1q, **8q**, **20q**, loss: 16q
Waldman et al, 2001	Tubular carcinoma	gain: 1q, **16p**, loss: 16q, **8p**
Thor et al, 2002	Invasive micropapillary carcinoma	gain: 1q, **8q**, **16p**, **17q**, loss: **8p**, 16q, **17p**
Nishizaki et al, 1997b	Primary and metastatic carcinoma	gain: 1q, **8q**, **17q**, loss: **6q**, 9q, **13q**, 16q, **17p**, **Xp**

TOTAL gain: 1q, **1p**, 4q, **5p**, **5q**, 6p, 6q, **8q**, **11q**, **12q**, **13q**, **16p**, **17q**, **19p**, **19q**, **20q**;   loss: **3p**, **6q**, **8p**, **9p**, **9q**, 11q, 12q, **13q**, 16q, **17p**, **18q**, **Xq**, **Xp**
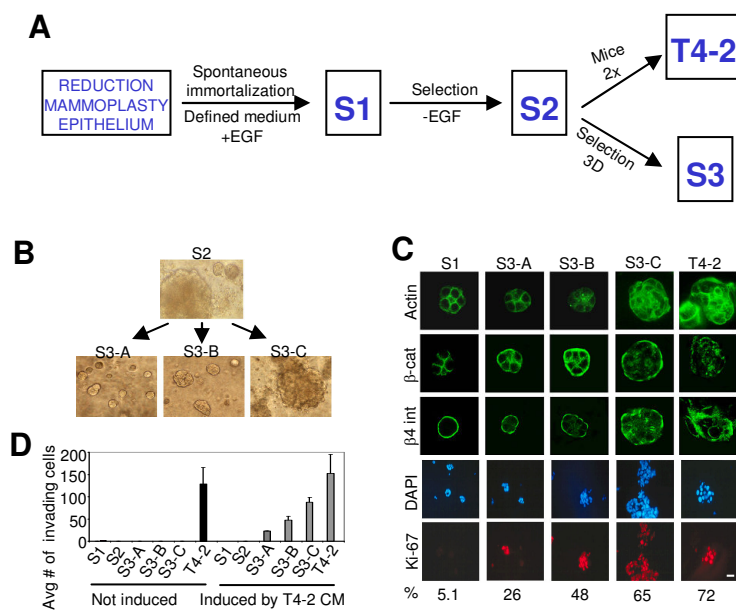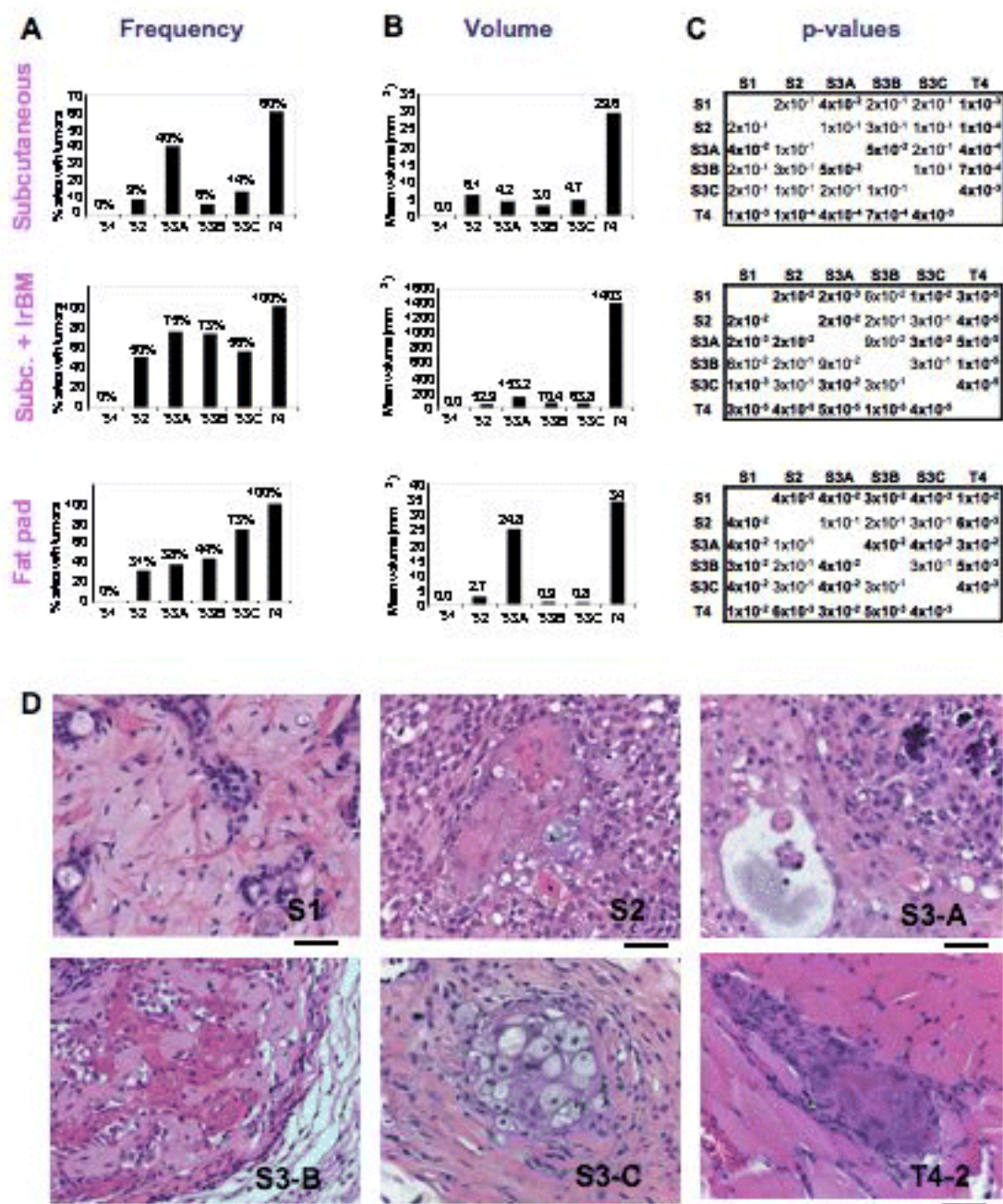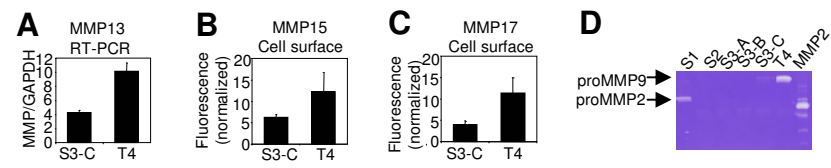
Figure 4.

Figure 5.

A

B

T4-2

C

T4-2

D

S3-C